Impact of helium and hydrogen plasma exposure on surface damage and erosion of tungsten

Ryuichi Sakamoto[1], **Elodie Bernard**[2], **Arkadi Kreter**[3], **Céline Martin**[4]

[1] National Institute for Fusion Science, Toki, Gifu 509-5292, Japan
[2] CEA, IRFM, F-13108 Saint-Paul-lez-Durance, France
[3] Forschungszentrum Jülich GmbH, Institut für Energie- und Klimaforschung - Plasmaphysik, 52425 Jülich, Germany
[4] Université Aix-Marseille, PIIM, 13397 Marseille, France

E-mail: sakamoto@nifs.ac.jp

August 2023

Abstract. The impact of helium plasma exposure on the tungsten surface damage structure development and erosion has been investigated by comparing the impact of hydrogen plasma exposure. Crystal orientation dependence of the undulating surface structure formation and erosion rate is observed on the plasma-exposed tungsten surface independently from the plasma species. The crystal orientation dependence of the undulating surface structure has been identified by a transmission method of the Electron backscatter diffraction measurements. The top surface of the plasma exposed tungsten has a tendency to be {100} plane independently from the initial surface orientation. Although hydrogen and/or helium cause no erosion in tungsten under incident ion energy exposure conditions below the sputtering threshold, inevitable minute impurities, like oxygen, play an essential role in erosion, and significant erosion can be observed even at 30 eV.

Submitted to: *Nucl. Fusion*

1. Introduction

In a magnetically confined fusion reactor that will use a deuterium-tritium reaction, tungsten is a primary candidate for plasma-facing materials due to its excellent high-temperature properties, high sputtering threshold energy, and low hydrogen retention and acceptable induced radioactivity [1]. Even in the first wall, where the magnetic field lines are not connected directly with high-temperature plasma, the plasma-facing materials are exposed to radiation and charge exchange particles from the core plasma and also exposed to scrap-off-layer plasma. The incident particles are not only fuel hydrogen isotope, but also several % of helium ash and the other impurities, and the total flux is estimated as $10^{20} - 10^{22}$ /m^2/s [2]. From the viewpoint of the protection

of a blanket under the first wall, the first wall must be thick and robust. On the other hand, from the viewpoint of the reasonable tritium breeding ratio (TBR) in a blanket, a thick first wall will not be allowed in order to minimize neutron attenuation. As a mutual compromise, only a thin tungsten coating layer which is sub-mm to a few mm thick is envisaged as the first wall to protect the blanket from the incident heat and particles [3, 4]. Therefore the erosion rate of tungsten is a critical issue not only for the lifetime of the plasma-facing materials but also for the TBR and lifetime of the blanket.

A considerable number of studies have been carried out on tungsten as a plasma-facing material from the viewpoint of both theoretical and experimental aspects for more than a decade [5, 6]. Many studies have shown strong impacts of helium exposure on mechanical properties and surface modification of tungsten, i.e., surface hardening, bubble, hole, and fuzz nanostructures [7–12]. And also, hydrogen isotope retention is significantly affected by the presence of helium in the tungsten surface layer [13]. This previous result motivates us to investigate helium exposure effects.

In the previous helium plasma exposure experiments, we have indicated the formation of a nano-scale undulating surface structure which shows a crystal orientation dependence and effective erosion even at low energy below the sputtering threshold [14, 15]. This paper investigates the impacts of helium plasma exposure on developing tungsten surface damage structure and erosion by comparing the impact of hydrogen plasma and hydrogen/helium mixed plasma exposure.

2. Experimental setup

High-purity tungsten ($>$ 99.995 %, Toho Kinzoku Co. Ltd) samples were mechanically mirror-polished and then annealed at 1773 K under low-pressure high-purity hydrogen conditions ($>$ 99.995 %, 0.03 MPa) for 2 hours to obtain a several 10 μm grain without surface oxidation layer for the surface analyses.

Pure hydrogen, pure helium, and hydrogen/helium mixed plasma exposure experiments have been carried out in the linear device PSI-2 [16]. The incident energy to the sample has been varied between 30 to 200 eV by adjusting the bias voltage. A radially scanning Langmuir probe is employed to measure plasma parameters, namely, electron density, electron temperature, space potential, and ion flux. Typical value of these parameters were 1.0×10^{18} /m^3, 9 eV, -20 V and 0.6×10^{22} /m^2/s, respectively. The plasma exposure experiment has been carried out up to an ion fluence of 1.0×10^{26} /m^2. The sample temperature is actively controlled at 773 K by a combination of water cooling and electric heating in addition to plasma heating based on an infrared (IR) camera temperature measurement with the support of thermocouple measurements.

After the plasma exposure experiments, the surface erosion and nanostructure development have been analyzed using diverse methods, such as scanning electron microscopy (SEM), transmission electron microscopy (TEM), confocal laser microscopy (CLM), electron backscatter diffraction (EBSD), and precision microbalance with an accuracy of 1 μg. A focused ion beam (FIB) method was employed to fabricate cross-

sectional samples for the depth profile observation of the damaged structure and surface morphology.

3. Result and discussion

3.1. Undulating surface structure

In the series of pure helium plasma exposure experiments in PSI-2, the nano-scale undulating surface structure, which shows crystal orientation dependence, is typically observed at temperatures below fuzz formation threshold [14, 15]. Near the {100} surface, the undulating surface structure cannot develop. As a grain surface tilt from the {100} surface, the interval of the undulating surface structure becomes narrower. A possible explanation for the undulating surface structure formation is that the top surface of the undulation tends to be {100} plane independently of the original surface orientation as shown in figure 10 of the reference [15]. To verify the relationship between the original surface orientation and the top surface of the undulation, EBSD measurements are applied to the cross-sectional sample, which is fabricated by using FIB processing. Figure 1 (a) shows an SEM image of helium plasma exposed tungsten surface at a fluence of 1×10^{26} /m^2. A cross-sectional sample was fabricated along the white line, which crosses the two-grain boundaries. Therefore, three grains, i.e., Grain A, B, and C, are included in the cross-section. Enlarged images of the undulating surface structure on each grain are also shown at the bottom of figure 1 (a). Figure 1 (b) shows crystal orientation which is measured by EBSD at the cross-section. The measured crystal orientation of each grain is shown by the cube. The cubes which show crystal orientations are also indicated in the enlarged surface images in figure 1 (a). One of {100} planes which is indicated by the gray color, corresponds to the top surface of the undulation in all grains. This observation result is evidence that the top surface of the undulation tends to be {100} plane independently of the original surface orientation.

3.2. Damage structure formation under hydrogen and helium plasma exposure

To verify the role of helium in the undulating surface structure formation, hydrogen, and helium mixed hydrogen plasma exposure experiments have been carried out comparatively. SEM images of the pure-hydrogen, helium-hydrogen mixture, and pure-helium plasma exposed tungsten surface at a fluence of 1×10^{26} /m^2 are shown in figure 2. The undulating surface structure, which has a different structure from grain to grain, is formed not only at pure-helium or helium-mixed plasma exposed surface but also at pure-hydrogen exposed surface. It becomes clear that the undulating surface structure is not the peculiar effect of the helium plasma exposure but the common effect of the plasma exposure because similar undulating surface structures are formed in the pure-hydrogen plasma. However, it should be noted that there is a clear difference between hydrogen plasma exposure and helium-contained plasma exposure in hole structure formation, which is developed from the aggregation of the helium bubble. Figure 3

shows SEM images of pure hydrogen plasma and helium 50 % mixed plasma exposed tungsten {100} surface where the undulating surface structure is not formed. The hole structure, which is $\sim$ 10 nm size black dot in SEM images, is never observed under pure hydrogen plasma exposure. However, it is a common damage structure under plasma exposures in which helium exists. Since the hole structure is formed by reaching the aggregated helium bubbles to the surface, the bubbles are not observed under the pure hydrogen exposure condition in the cross-sectional TEM observation, as shown in figure 4.

3.3. Surface erosion enhancement with impurity

From the comparison between hydrogen plasma and helium plasma exposure, an essential role of helium exposure is the formation of bubble and hole structures. But there is no further visible effect from the surface observations with SEM and TEM. On the other hand, erosion enhancement with helium exposure is still possible because flaking, which may lead to mass loss, is observed as associated with the hole structure development [15]. Mass losses are measured by comparing mass differences before and after the plasma exposure experiments under various plasma exposure conditions to verify the helium effects on erosion enhancement. Figure 5 shows an incident energy dependence of the erosion amounts at a fluence of 1×10^{26} /m^2. The circle and square symbols denote the measured erosion amount with helium and hydrogen plasma exposure, respectively. Even though the range of incident energy of the plasma particles is lower than the threshold energies of tungsten sputtering (H: $\sim$ 500 eV, He: $\sim$ 110 eV), the erosion can be observed generally in both helium and hydrogen plasma exposure experiments. In our experiments, measurable erosions are observed under all experimental conditions down to 33 eV. Another important finding is that there is no significant difference between hydrogen plasma and helium plasma in erosion amount. Especially at 70 eV, there is almost the same erosion amount among pure hydrogen, 10 % helium mixed, and 50 % helium mixed plasma exposure. The results mentioned above imply that the major operation gas, i.e., helium and hydrogen, have no impact on the tungsten erosion, but inevitable minute impurities, e.g., oxygen, play an essential role in erosion. The tungsten erosion with oxygen ion has been estimated from the database of the sputtering yield [17]. Since the sputtering yield database is based on the monovalent ion, it is required to compensate for incident energy considering the multivalent ion fraction in plasma. Although the plasma electron temperature and density are measured by using a Langmuir probe in our experiments, a large perpendicular anomalous transport [18] makes it difficult to estimate the multivalent ion fraction by assuming an equilibrium state. Here, the temperature dependence of the multivalent ion fraction, which was measured by the Mass-spectrometer of magnetized plasmas (MSMP-03) [19] is applied to estimate the multivalent ion fraction. The MSMP-03 measurements show that the ratio of $He^{2+}/(He^{+}+He^{2+})$ decreases as the electron temperature decreases, and the ratio is 0.4 % at 10 eV electron temperature. In our

experiments, therefore, the ratio of $He^{2+}/(He^{+}+He^{2+})$ is not more than 0.4 % because a typical electron temperature is 9 eV. Since there are no measurements on the multivalent ion fraction of oxygen, the neon data is used for a rough estimation considering the similar ionic fraction in the equilibrium state [20]. Here, the ratio of $O^{2+}/(O^{+}+O^{2+})$ is assumed as 10 % considering the ratio of $Ne^{2+}/(Ne^{+}+Ne^{2+})$ which is measured by the MSMP-03 measurements. Since measuring the minute oxygen content in the plasma is difficult, the oxygen content rate is set as a fitting parameter for reproducing experiment results.

The thick solid line and thick dashed line denote incident energy dependences of the total calculated erosion amount for hydrogen and helium plasma, which include erosion enhancement effect with the 0.13 % oxygen impurity, and the dotted and dashed thin lines denote one of each consistent elements, namely, H^{+}, He^{+}, He^{2+}, O^{+} and O^{2+}. Under low incident energy conditions below the sputtering threshold energy of the main operational gas, the erosion amounts are governed by oxygen impurity independently from the main operational gas, namely, hydrogen and helium. It should note that the discrepancy between measured and calculated erosion becomes prominent, as shown by the arrow in the high energy region above the sputtering threshold energy ($\sim$ 110 eV) in the helium plasma exposure. These observations imply that a selective sputtering reduction, namely, the sputtering only by helium is reduced while the sputtering by oxygen is kept. As shown by the thick dotted line, only the helium sputtering yield must be reduced to 1/10 in the erosion calculation to reproduce the experimental observation. A possible explanation of the selective sputtering reduction is due to a range of incident particles. The range and peak of 200 eV helium in tungsten are 8.1 nm and 2.6 nm, respectively, by TRIM code [21]. And the range of helium overlaps with the bubble formative layer in Figure 4 (b). A numerical simulation shows a reduction of sputtering yield in the presence of a helium bubble because incident helium atoms tended to stop in bubbles transferring their kinetic energy efficiently to the helium atom of the same mass [22]. On the other hand, the range and peak of 200 eV oxygen are as shallow as 0.9 nm and 3.9 nm, in which there are no large bubbles. Therefore, there is no reduction of sputtering yield with oxygen impurity, even in the presence of a helium bubble. Comparative experiments with hydrogen plasma exposure may be helpful to verify this working hypothesis because there is no bubble formation in the hydrogen plasma exposure. Nevertheless, it is not clear whether there is a similar effect in the hydrogen plasma exposure because the sputtering threshold energy ($\sim$ 440 eV) is sufficiently higher than the range of the experiments ($<$ 200 eV). And therefore, the erosion should be fully governed by the inevitable minute impurities.

4. Summary

Under heavy plasma exposure beyond the fluence of 1×10^{26} /m^2 in the temperature range below the fuzz formation threshold, the top surface of tungsten tends to be {100} plane independently of the original surface orientation. Consequently, the undulating

surface structure, which shows crystal orientation dependence, is formed on the plasma-exposed surface. It becomes clear that the undulating surface structure is not the peculiar effect of the helium plasma exposure but the common effect of the plasma exposure because similar undulating surface structures are formed in the pure-hydrogen plasma. The clear difference between hydrogen plasma exposure and helium-contained plasma exposure is the formation of bubbles and holes, which are developed from the aggregation of the helium bubbles.

The tungsten erosion under hydrogen and helium plasma exposure is governed by inevitable minute impurities like oxygen in the energy region below the sputtering threshold of hydrogen and helium, and significant erosion can be observed even at 30 eV. The helium bubble may selectively reduce the erosion with helium plasma exposure, although further exposure experiments at higher incident energy are required to confirm this.

Acknowledgments

The authors are grateful to the staff of the PSI-2 team for their experimental support and to Mr. D. Nagata for preparing the TEM samples. This work is supported by the IEA Technology Collaboration Programme on the Development and Research on Plasma Wall Interaction Facilities for Fusion Reactors (PWI TCP).

References

[1] G. Pintsuk, "Tungsten as a plasma-facing material", Reference Module in Comprehensive Nuclear Materials, Vol. 4, pp. 551-581 (2012). http://doi.org/10.1016/B978-0-08-056033-5.00118-X

[2] K. Hoshino, N. Asakura, S. Tokunaga, Y. Homma, K. Shimizu, Y. Sakamoto, K. Tobita, Joint Special Design Team for Fusion DEMO, "Physics design study of the divertor power handling in 8 m class DEMO reactor", Fusion Engineering and Design 124 (2017) 352-355. http://doi.org/10.1016/j.fusengdes.2017.03.068

[3] Y. Someya, K. Tobita, H. Utoh, S. Tokunaga, K. Hoshino, N. Asakura, M. Nakamura, Y. Sakamoto, "Design study of blanket structure based on a water-cooled solid breeder for DEMO", Fusion Engineering and Design 98-99 (2015) 1872-1875. http://doi.org/10.1016/j.fusengdes.2015.05.042

[4] P. Pereslavtsev, C. Bachmann and U. Fischer, "Neutronic analyses of design issues affecting the tritium breeding performance in different DEMO blanket concepts", Fusion Engineering and Design 109 (2016) 1207-1211. http://doi.org/10.1016/j.fusengdes.2015.12.053

[5] J. Roth, E. Tsitrone, A. Loarte, T. Loarer, G. Counsell, R. Neu, V. Philipps, S. Brezinsek, M. Lehnen, P. Coad, Ch. Grisolia, K. Schmid, K. Krieger, A. Kallenbach, B. Lipschultz, R. Doerner, R. Causey, V. Alimov, W. Shu, O. Ogorodnikova, A. Kirschner, G. Federici, A. Kukushkin, "Recent analysis of key plasma wall interactions issues for ITER", Journal of Nuclear Materials 390-391 (2009) 1-9. http://doi.org/10.1016/j.jnucmat.2009.01.037

[6] B.D. Wirth, K.D. Hammond, S.I. Krasheninnikov, D. Maroudas, "Challenges and opportunities of modeling plasma-surface interactions in tungsten using high-performance computing", Journal of Nuclear Materials 463 (2015) 30-38. http://doi.org/10.1016/j.jnucmat.2014.11.072

[7] E. Lucon, P. Benoit, P. Jacquet, E. Diegele, R. Lässer, A. Alamo, R. Coppola, F. Gillemot, P. Jung, A. Lind, S. Messoloras, P. Novosad, R. Lindau, D. Preininger, M. Klimiankou, C.

Petersen, M. Rieth, E. Materna-Morris, H.-C. Schneider, J.-W. Rensman, B. van der Schaaf, B.K. Singh, P. Spaetig "The European effort towards the development of a demo structural material: Irradiation behaviour of the European reference RAFM steel EUROFER", Fusion Engineering and Design 81 (2006) 917-923. http://doi.org/10.1016/j.fusengdes.2005.08.044

[8] S. Kajita, W. Sakaguchi, N. Ohno, N. Yoshida and T. Saeki, "Formation process of tungsten nanostructure by the exposure to helium plasma under fusion relevant plasma conditions", Nuclear Fusion 49 (2009) 095005. http://doi.org/10.1088/0029-5515/49/9/095005

[9] G. De Temmerman, K. Bystrov, J.J. Zielinski, M. Balden, G. Matern, C. Arnas and L. Marot, "Nanostructuring of molybdenum and tungsten surfaces by low-energy helium ions", Journal of Vacuum Science & Technology A 30 (2012) 041306. http://doi.org/10.1116/1.4731196

[10] M.J. Baldwin, R.P. Doerner, "Helium induced nanoscopic morphology on tungsten under fusion relevant plasma conditions", Nuclear Fusion 48 (2008) 035001. http://doi.org/10.1088/0029-5515/48/3/035001

[11] S. Takamura and Y. Uesugi, "Experimental identification for physical mechanism of fiber-form nanostructure growth on metal surfaces with helium plasma irradiation", Applied Surface Science 356 (2015) 888-897. http://doi.org/10.1016/j.apsusc.2015.08.112

[12] M. Miyamoto, S. Mikami, H. Nagashima, N. Iijima, D. Nishijima, R.P. Doerner, N. Yoshida, H. Watanabe, Y. Ueda, A. Sagara, "Systematic investigation of the formation behavior of helium bubbles in tungsten", Journal of Nuclear Materials 463 (2015) 333-336. http://doi.org/10.1016/j.jnucmat.2014.10.098

[13] E. Bernard, R. Sakamoto, A. Kreter, M. F. Barthe, E. Autissier, P. Desgardin, H. Yamada, S. Garcia-Argote, G. Pieters, J. Chêne, B. Rousseau and C. Grisolia, "Tungsten as a plasma-facing material in fusion devices: impact of helium high-temperature irradiation on hydrogen retention and damages in the material", Physica Scripta T170 (2017) 014023. http://doi.org/10.1088/1402-4896/aa89f7

[14] R. Sakamoto, E. Bernard, A. Kreter, N. Yoshida, "Surface morphology of tungsten exposed to helium plasma at temperatures below fuzz formation threshold 1073 K," Nuclear Fusion 57 (2016) 016040. http://doi.org/10.1088/1741-4326/57/1/016040

[15] R. Sakamoto, E. Bernard, A. Kreter, C. Martin, B. Pégourié, G. Pieters, B. Rousseau, C. Grisolia, N. Yoshida, "Surface morphology in tungsten and RAFM steel exposed to helium plasma in PSI-2", Physica Scripta T170 (2017) 014062. http://doi.org/10.1088/1402-4896/aa93a2

[16] A. Kreter, C. Brandt, A. Huber, S. Kraus, S. Möeller, M. Reinhart, B. Schweer, G. Sergienko and B. Unterberg, "Linear Plasma Device PSI-2 for Plasma-Material Interaction Studies", Fusion Science and Technology 68 (2015) 8-14. http://doi.org/10.13182/FST14-906

[17] R. Behrisch and W. Eckstein, "Sputtering by Particle Bombardment", Springer (2007).

[18] O. Waldmann, H. Meyer, G. Fussmann, "Anomalous diffusion in a linear plasma generator", Contributions to Plasma Physics 47 (2007) 691-702. http://dx.doi.org/10.1002/ctpp.200710079

[19] I. A. Sorokin, I. V. Vizgalov, V. A. Kurnaev, C. Brandt, A. Kreter, C. Linsmeier, "In-situ mass-spectrometer of magnetized plasmas" Nuclear Materials and Energy 12 (2017) 1243-1247. http://dx.doi.org/10.1016/j.nme.2017.01.015

[20] M. Arnaud, R. Rothenflug, "An updated evaluation of recombination and ionization rates", Astronomy & Astrophysics Supplement Series 60 (1985) 425-457.

[21] J. F. Ziegler, J. P. Biersack and M. D. Ziegler, "The Stopping and Range of Ions in Solids", www.SRIM.org (2008)

[22] S. Saito, H. Nakamura, M. Tokitani, R. Sakaue and K. Yoshida, "Determination of dynamical changes in sputtering and retention on bubble-growing tungsten under helium plasma irradiation by binary-collision-approximation-based simulation", Japanese Journal of Applied Physics 55 (2016) 01AH07. http://doi.org/10.7567/JJAP.55.01AH07

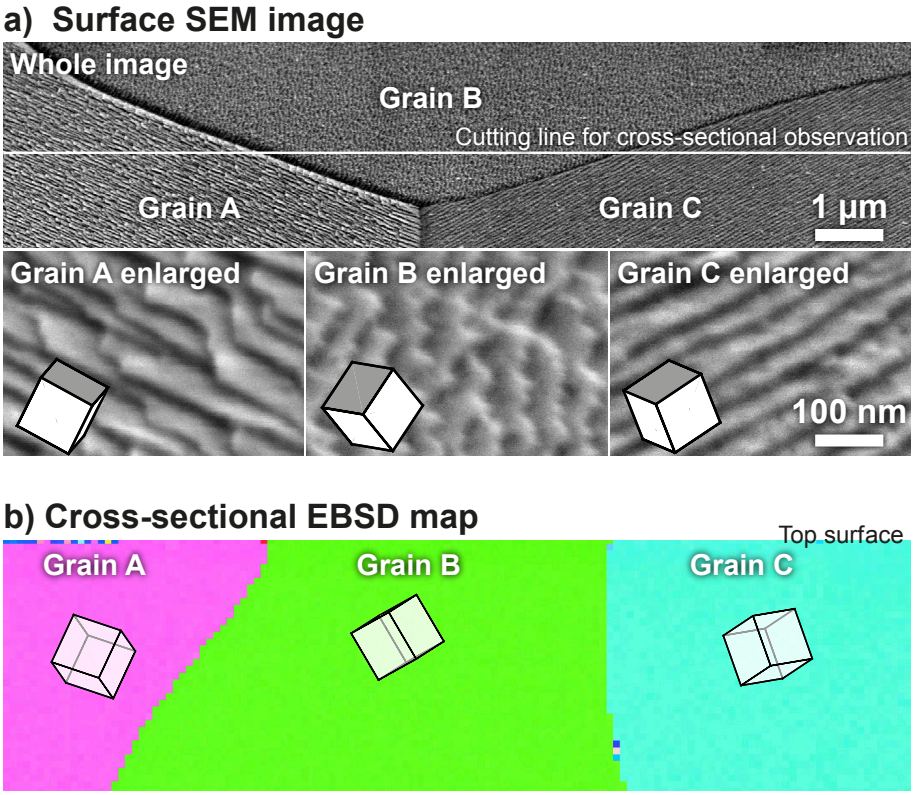

Figure 1. (a) SEM image of helium plasma exposed tungsten surface at a fluence of 1×10^{26} /m^2. The top image shows the whole image before making the cross-sectional sample. The white line indicates the cutting line for fabricating the cross-sectional sample. The bottom three images are enlarged images of each grain and projected crystal orientations, which are measured by EBSD. (b) Cross-sectional EBSD map and measured crystal orientation in each grain.

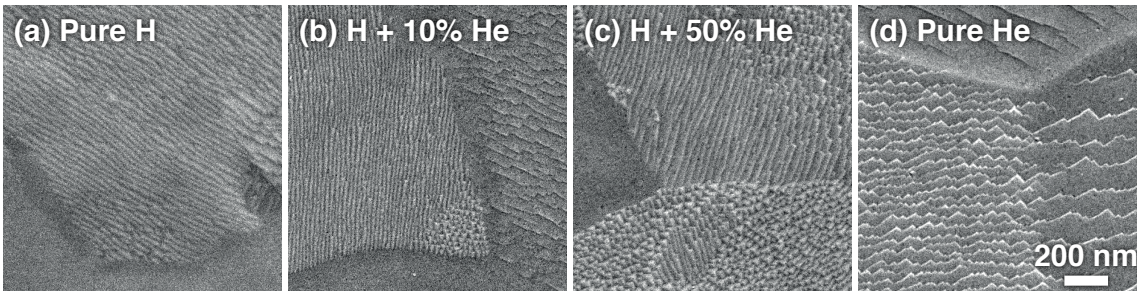

Figure 2. SEM images of (a) pure hydrogen plasma, (b) 10 % helium mixed hydrogen plasma, (c) 50 % helium mixed hydrogen plasma and (d) pure helium plasma exposed tungsten surface at a fluence of 1×10^{26} /m^2.

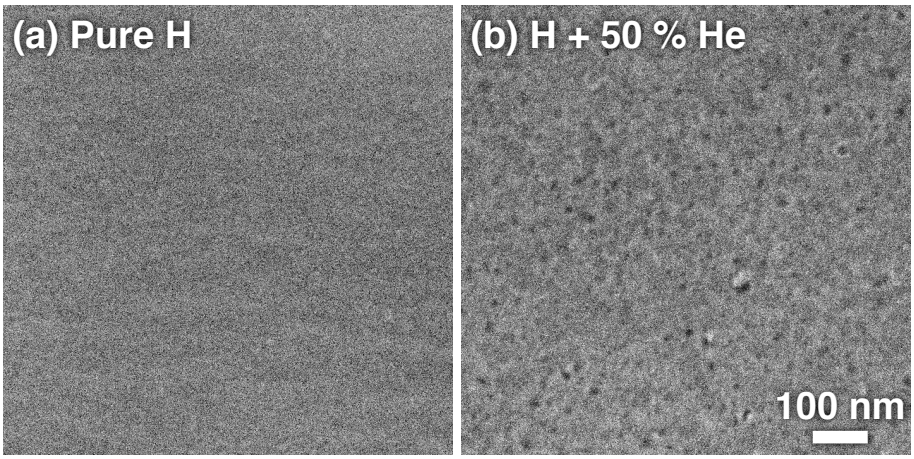

Figure 3. SEM images of (a) pure hydrogen plasma and (b) 50 % helium mixed hydrogen plasma exposed tungsten {100} surface at a fluence of 1×10^{26} /m^2.

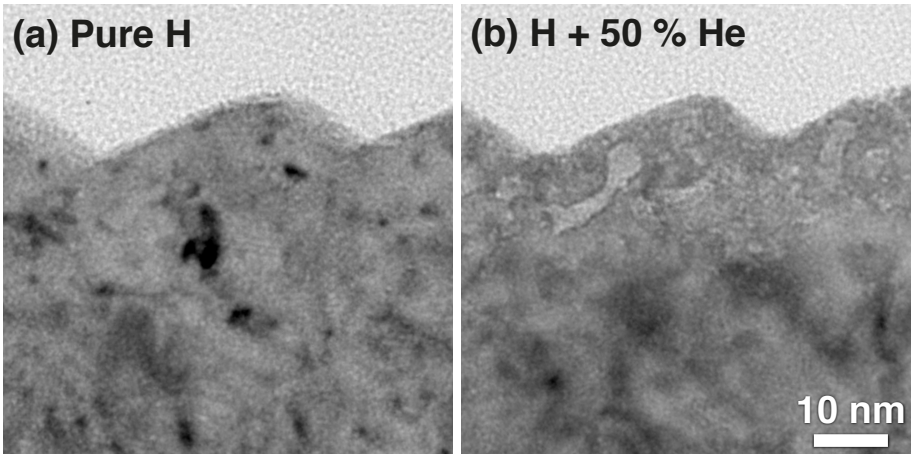

Figure 4. Cross-sectional TEM images of (a) pure hydrogen plasma and (b) 50 % helium mixed hydrogen plasma exposed tungsten at a fluence of 1×10^{26} /m^2.

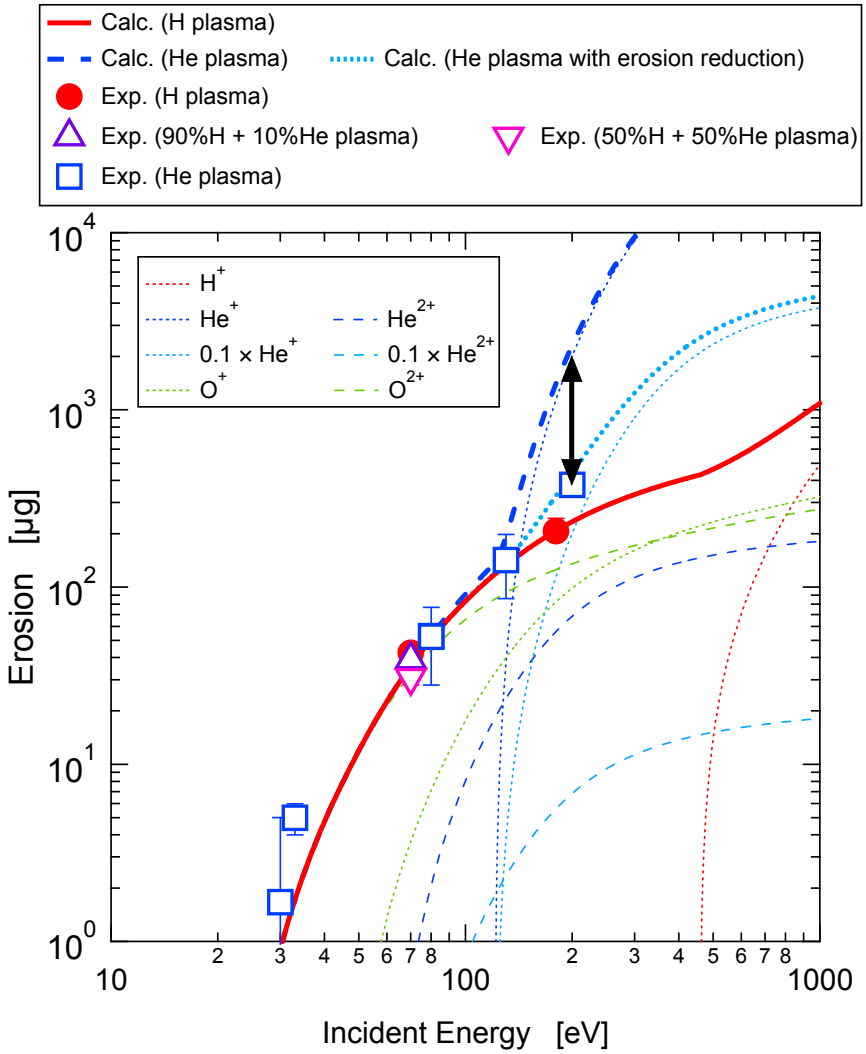

Figure 5. Incident energy dependence of the erosion amount at a fluence of 1×10^{26} /m^2. The circle, square, and triangle symbols denote the measured erosion amount with hydrogen, helium, and their mixed plasma. The thick lines denote calculated global erosion, and the thin lines denote partial erosion by plasma components, i.e., hydrogen, helium, and oxygen ions.